

## Quantum-Noise-Initiated Symmetry Breaking of Spatial Solitons

S. D. Jenkins,<sup>1,2</sup> D. Salerno,<sup>2,3</sup> S. Minardi,<sup>4,5</sup> G. Tamošauskas,<sup>6</sup> T. A. B. Kennedy,<sup>1,2</sup> and P. Di Trapani<sup>2</sup>

<sup>1</sup>*School of Physics, Georgia Institute of Technology, Atlanta, Georgia 30332-0430, USA*

<sup>2</sup>*Dipartimento di Fisica e Matematica, Università dell'Insubria, Via Valleggio 11, 22100 Como, Italy*

<sup>3</sup>*Dipartimento di Fisica, Università degli studi di Milano, Via Celoria 16, 20133 Milano, Italy*

<sup>4</sup>*ICFO - Institut de Ciències Fotòniques, Jordi Girona 29, NEXUS II, E-08034 Barcelona, Spain*

<sup>5</sup>*Technical Educational Institute of Crete, Romanou 3, GR-73122 Chania, Greece*

<sup>6</sup>*Department of Quantum Electronics, Vilnius University, Saulėtekio Avenue 9, Building 3, LT-10222 Vilnius, Lithuania*

(Received 11 May 2005; published 7 November 2005)

The spectra of  $\chi^{(2)}$  spatial solitons are measured close to the soliton-formation threshold and show the presence of sidebands, shifted by 39 THz from the laser line. By comparing with the predictions of a quantum optical field model, solved numerically in the full  $(3 + 1)$ -dimensional space, it is claimed that the observed temporal instability of the spatial soliton is seeded by vacuum state fluctuations of the electromagnetic field.

DOI: [10.1103/PhysRevLett.95.203902](https://doi.org/10.1103/PhysRevLett.95.203902)

PACS numbers: 42.65.Tg, 42.50.Lc, 42.65.Ky, 42.65.Sf

The breakup or collapse of a macroscopic order parameter, or mean field, is one of the more dramatic effects caused by quantum fluctuations. By its very nature it implies intrinsic instability even under conditions of optimum experimental purity. The initiation of a mean field breakup is, however, often masked by the difficulty in clearly establishing the quantum origins of the process: a pencil balanced on its point may be induced to fall by quantum-noise, but once it tips, the fluctuation's origin is lost in an essentially classical collapse [1,2]. In this Letter we report experimental and theoretical investigations of quantum-noise-initiated temporal breakup of a macroscopic coherent spatial structure: an optical soliton self-localized in two transverse spatial dimensions in a nonlinear medium. Specifically, we experimentally measure a symmetry breaking instability in the temporal dimension of the spatial solitary wave, induced by zero point fluctuations of the electromagnetic vacuum.

The general problem of soliton symmetry breaking or modulational instability (i.e., the instability with respect to a perturbation in a spacetime dimension other than those in which the soliton is localized) was initially formulated in a classical context for the nonlinear Schrödinger equation by Zakharov [3]. In this Letter we discuss soliton generation *via* second harmonic generation in a  $\chi^{(2)}$  bulk medium [degenerate three wave mixing (DTWM) in the normal dispersion regime]. The symmetry breaking of 1D  $\chi^{(2)}$  solitons, or solitary waves, was discussed theoretically by Kanashov and Rubenchik [4], and a prediction of symmetry breaking for 2D  $\chi^{(2)}$  spatial solitons in DTWM was made by De Rossi *et al.* [5]. From the latter work, one expects to observe a narrow band, regular, temporal modulation of the 2D soliton, characteristic of modulational instability. To our knowledge, no experimental evidence of such temporal modulation, or measurements of the spectral profile of 2D  $\chi^{(2)}$  spatial solitons has been reported previously [6]. To observe this effect it is favorable to work

in the regime of positive wave vector mismatch, since for negative mismatch Skryabin [7] has shown, for the case of 1D spatial solitons, that overlapping instability branches lead to a broadband gain profile. In that case, as well as in the case of instabilities excited in parametric down conversion, one should expect a chaotic breakup of the wave packet in the spatiotemporal domain [8], completely different from the situation studied here, namely, that of genuine symmetry breaking of a *spatial* object in the *temporal* domain.

While the observation of a temporal instability of a 2D spatial soliton is novel even in a completely classical context, we contend that the observed breakup is initiated by quantum noise. As a matter of principle it is, therefore, unavoidable. It is usually the case that observed modulational instabilities are seeded by classical noise, perhaps due to residual stochastic fluctuations of the input laser field, or imposed by some technical laboratory source. In addition to such noise, quantum fluctuations of the vacuum are always present, but this is a source which is often considered harmless for high intensity light fields. The peculiarity of our DTWM experiment is that the chosen boundary conditions force the instability to appear in a spectral region where classical noise should be readily excluded. The good agreement between the experimental results and the predictions of a quantum optical model further supports our claim.

The experiment has been designed to capture the growth of frequency sidebands in the soliton temporal spectrum near the soliton-formation threshold, and to precisely measure their energy content in order to allow comparison with model predictions. A 1.2 ps FWHM duration, 32  $\mu\text{m}$  FWHM diameter, 1055 nm wavelength optical pulse delivered by a chirped-pulse amplified Nd:glass laser (TWINKLE; Light Conversion Ltd.) was launched into a 30 mm lithium triborate (LBO) crystal, where spatial solitons are formed owing to the interaction between the input fundamental (FH) and generated second harmonic

(SH) fields. The input-beam waist was placed at the crystal input facet, and the pulse energy varied in the 0–1  $\mu\text{J}$  range. The crystal temperature was kept at 166.4  $^{\circ}\text{C}$ , supporting noncritical phase matching with small, positive, phase mismatch (+5  $\text{cm}^{-1}$ ).

The experimental diagnostic consisted of three different apparatus: (i) a 12-bit CCD detector with 4x magnifying optics was adopted for recording the FH and SH beam profiles at the crystal output facet, as required for identifying the occurrence of the soliton regime. (ii) A spectrograph configured as scanning monochromator was used for detecting the blue-shifted sideband spectral profile. To this end the LBO crystal output facet was imaged (with 4 $\times$  magnification) onto the entrance slit of the spectrograph, whose aperture was set to 1 mm in order to accept the entire beam and to make negligible any beam-wandering effect. This setting limited the spectral resolution to 10 nm. The acquisition was performed by means of low-noise photodiodes. (iii) Finally, by opening the spectrograph output slit to 4 mm (spectral width: 40 nm, corresponding to  $\approx 15$  THz at 930 nm), virtually the entire sideband energy was recorded on the photodiode for a single grating position, as we have verified by further increasing slit aperture. This setting was used to record the ratio between the blue-shifted-sideband energy,  $E_{\text{SB}}$ , centered at 930 nm, and the energy of the residual output FH,  $E_{\text{FH}}$ , i.e., that contained in the same 40 nm bandwidth centered at 1055 nm. The red-shifted sideband, centered at 1219 nm, was not recorded.

Figure 1(a) shows the FH output-beam FWHM diameters vs the threshold-normalized input-pump energy,  $E_p/E_{\text{TH}}$ . The trend, similar to that shown in Ref. [9], demonstrates the occurrence of the spatial-soliton regime;  $E_{\text{TH}}$ , defined as the pump energy with the minimum FH output diameter, occurred for  $E_p = 0.44$   $\mu\text{J}$ . Figure 1(b) presents, in arbitrary units, the measured spectra (FH branch, blue-shifted side) for four different input energies close to the soliton-formation threshold. The results clearly outline the emergence of a well-defined frequency sideband in the

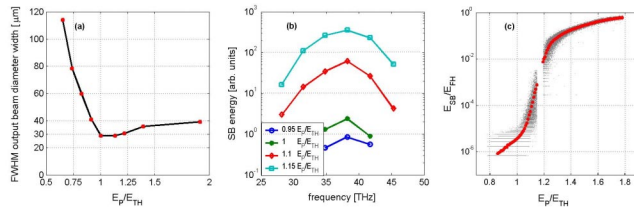


FIG. 1 (color online). Experimental results. (a) FWHM diameter of the FH output-beam vs threshold-normalized input-pump energy,  $E_p/E_{\text{TH}}$ ; (b) spectral-density profiles of the blue-shifted sidebands close to soliton-formation threshold; (c) dependence of the fractional blue-sideband energy,  $E_{\text{SB}}/E_{\text{FH}}$ , on normalized pump energy. The (60 000) scattered points represent measured data, while the squared symbol result from data averaging over 0.25  $\text{GW}/\text{cm}^2$  windows. The two branches of the curve were obtained with two sets of neutral-density filters, in order to cover the largest possible dynamic range.

temporal spectrum, which proves the occurrence of spatial-soliton instability in the temporal domain. The above-threshold sidebands have a width (at 1/10 of their peak) of  $\approx 15$ –20 THz, and are peaked at  $\approx 39$  THz from the pump. We note that our Nd:glass laser has a stretcher and compressor, which ensure a sharp laser noise cutoff of less than 2 THz for the input pulses. To assess whether the residual classical noise could be responsible for the observed instability, we use Eqs. (1) and (2) supplemented by an Ornstein-Uhlenbeck model of laser phase noise specified by two frequency parameters  $b$  and  $\beta$  [10]. We do not expect that the qualitative results should depend sensitively on the model. Furthermore, to account for the stretcher and compressor we numerically filter out frequencies above 2 THz. The results of simulations in the threshold region are shown in Fig. 2 for a range of noise parameters leading to the appearance of sidebands. Under conditions where laser noise broadening could produce near-threshold sidebands, the sideband energies are several orders of magnitude larger than those observed experimentally. Moreover, they appear without the distinctive spectral gap between sidebands and pump. In this scenario, excluding laser noise, quantum noise emerges as the key factor that triggers the observed spatial-soliton temporal instability, *via* the very efficient coupling supported by the  $\chi^{(2)}$  interaction. As to possible contributions of Kerr or Raman-driven instabilities, which might grow in principle as a consequence of the same quantum-noise seeding, it should be noted that they would have a much weaker gain than the  $\chi^{(2)}$  process. Spontaneous Raman photons, with a Stokes shift in the tens of THz range could be amplified by the  $\chi^{(2)}$  interaction in the same manner as the vacuum input; however, this process also has a distinctly quantum origin: the disappearance of a pump photon results in the appearance of a real Stokes photon in a previously unoccupied (vacuum) field mode. Figure 1(c) gives the measured sideband-energy content,  $E_{\text{SB}}/E_{\text{FH}}$ . The results show that the spatial

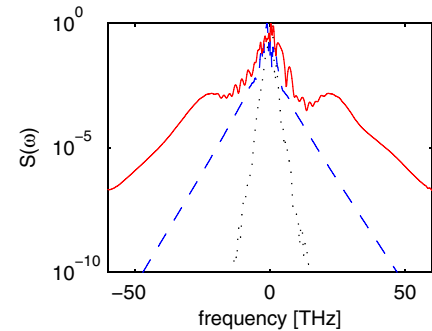


FIG. 2 (color online). Theoretical spectra,  $S(\omega) = \int dx dy S(\omega, x, y)$ , computed for pump energy  $E_p/E_{\text{TH}} = 1.1$ , showing the emergence of sidebands caused by classical laser noise. The noise parameters are given by  $b/2\pi = 0.4$  THz,  $\beta/2\pi = 2.0$  THz (dotted line),  $b/2\pi = 1.0$  THz,  $\beta/2\pi = 1.0$  THz (dashed line) and  $b/2\pi = 1.2$  THz,  $\beta/2\pi = 2.0$  THz (solid line).

soliton exhibits temporal modulation already at its formation threshold, and  $E_{SB}/E_{FH}$  takes a value of  $\approx 10^{-5}$  for  $E_p/E_{TH} = 1.1$ . Note that the first slope change around threshold is linked to the abrupt change in beam width and therefore to the effective pump intensity; the second, at  $E_p/E_{TH} = 1.2$ , is where saturation occurs.

We compute the quantum features of the instability using the methods of quantum optics. The Heisenberg field equations can be obtained by quantization of the classical field theory for DTWM [11–13]. The idea is then to recast these operator equations into stochastic partial differential equations using the Wigner function representation. The use of such an approach in nonlinear optics has been pioneered by Drummond and coworkers [12–15]. A similar approach in the context of Bose-Einstein condensation has also been advocated [16,17]. With respect to previous work, the novelty of our calculations is that they are fully  $3 + 1$  dimensional, taking into account the strong spatial and temporal reshaping of the coupled light fields and quantum fluctuations during propagation. We also account for the dominant effect of group velocity mismatch which was not considered in earlier theoretical and numerical discussions [5]. Details of the theory will be discussed elsewhere, and below we will summarize only the essential features. The essence of the model is that we make a Wigner function truncation approximation so that it reduces to the classical propagation equations and initial conditions that include noise whose properties are entirely determined by the quantum field theory.

The equations of motion are simplest in a frame comoving at the group velocity  $v_{g1}$  of FH, where in terms of laboratory space time coordinates  $(X, Y, Z, T)$  we define local coordinates,  $z_v = Z$ ,  $t_v = T - Z/v_{g1}$ . Furthermore, we normalize the equations through transformations to dimensionless variables:  $\mathbf{x} = (X, Y)/r_0 = \mathbf{X}/r_0$ ,  $\tau = t_v/t_0$ ,  $\zeta = z_v/z_0$ , and  $\phi_\mu = \Phi_\mu/F_0$ , where  $\Phi_\mu$  is the photon flux field in the Wigner representation analogous to the photon flux Heisenberg operator  $\hat{\Phi}_\mu$ . The characteristic photon flux  $F_0^2 = I_0/(\hbar\omega_0^{(1)})$  with  $I_0$  a characteristic intensity, which we will take to be the peak intensity of the input gaussian FH pulse of frequency  $\omega_0^{(1)}$ . The length and time scales are then given by  $z_0 = (F_0\chi)^{-1}$ ,  $r_0 = (z_0/k_0^{(1)})^{1/2}$ ,  $t_0 = (z_0|k_0^{(1)''}|)^{1/2}$ , where the scaled nonlinearity  $\chi \equiv [\chi^{(2)}k_0^{(1)}/(n_1^2n_2)]/[\hbar k_0^{(2)}/(2\epsilon_0)]^{1/2}$ ,  $k_0^{(\mu)}$  is the wave number of field  $\mu$ ,  $n_\mu$  is the index of refraction for field  $\mu$ , and the group velocity dispersion  $k_0^{(\mu)''} \equiv d^2k/d\omega^2|_{k=k_0^{(\mu)}}$ . The dimensionless field equations are given by

$$\frac{\partial}{\partial \zeta} \phi_1 = \left( -\frac{i}{2} s_1 \frac{\partial^2}{\partial \tau^2} + i \frac{1}{2} \nabla_{\mathbf{x}}^2 \right) \phi_1 - \phi_1^* \phi_2, \quad (1)$$

$$\frac{\partial}{\partial \zeta} \phi_2 = \left( \Delta \frac{\partial}{\partial \tau} - \frac{i}{2} s_2 \frac{\partial^2}{\partial \tau^2} + \frac{i}{2} \frac{k_0^{(1)}}{k_0^{(2)}} \nabla_{\mathbf{x}}^2 \right) \phi_2 - i \delta k \phi_2 + \frac{1}{2} \phi_1^2, \quad (2)$$

where  $s_1 = \text{sgn}(k_0^{(1)'')}$ ,  $s_2 = k_0^{(2)''} v_{g2}^2 / (|k_0^{(1)''}| v_{g1}^2)$ , the group velocity mismatch  $\Delta = z_0(1/v_{g1} - 1/v_{g2})/t_0$ , and the phase mismatch  $\delta k = (2k_0^{(1)} - k_0^{(2)})z_0$ . We assume the quantized field incident on the input face of the crystal,  $\zeta = 0$ , is a coherent state. In the Wigner representation, this coherent initial condition is represented by a classical field with a superposed white noise as in Refs. [13,15]; explicitly,  $\phi_\mu = \phi_\mu^0 + \delta\phi_\mu$  where the noise,  $\delta\phi_\mu(\tau, \zeta, \mathbf{r})$ , is a Gaussian random noise with zero mean whose correlations are fixed by the nonzero equal space commutation relations at  $\zeta = 0$ ,  $[1 \equiv (\tau_1, \mathbf{x}_1), \text{etc.}]$

$$\overline{\delta\phi_\mu(1)\delta\phi_\nu^*(2)} = \frac{1}{2\bar{n}} \frac{v_{g\mu}}{v_{g1}} \delta_{\mu\nu} \delta(\mathbf{x}_1 - \mathbf{x}_2) \delta(\tau_1 - \tau_2) \quad (3)$$

where  $\bar{n} = \Phi_0^2 r_0^2 t_0$  is a characteristic photon number.

We must recall that in using the Wigner function method, ensemble averages correspond to symmetrically ordered expectation values. For example, the FH space-frequency spectrum,  $S_1(\omega, \mathbf{x})$ , is the Fourier transform of the normally ordered quantity  $\langle \hat{\Phi}_1^\dagger(t_1, \mathbf{X}) \hat{\Phi}_1(t_2, \mathbf{X}) \rangle$ . In Wigner representation this is, up to a constant, the ensemble average of  $|\phi_1(\omega, \mathbf{x})|^2$  minus the limit of Eq. (3) ( $\mu = 1$ ) as  $\mathbf{x}_1 \rightarrow \mathbf{x}_2$  and  $\tau_1 \rightarrow \tau_2$ . Here  $\omega = \Omega t_0$  is a dimensionless frequency, and  $\phi_\mu(\omega, \mathbf{x})$  is the Fourier transform of  $\phi_\mu(\tau, \mathbf{x})$ . In practice all delta functions are regularized numerically as Kronecker delta symbols on the lattice.

The numerical calculations were carried out on a three dimensional spatiotemporal grid of size  $L_\tau L_x L_y$  with  $N_\tau N_x N_y$  points, and the values updated as the field propagates in the  $\zeta$  direction [18] with a step size small enough to ensure convergence  $\delta\zeta = 0.04$ . The quantum-noise input was treated by assigning independent noise to each point on the grid; for this reason the calculations are necessarily  $3 + 1$  dimensional. The variance of the noise on each grid point is thus proportional to  $1/\Delta V$  where  $\Delta V = L_\tau L_x L_y / N_\tau N_x N_y$  is the volume element associated with each grid point. The procedure is equivalent to adding noise equal to “half a photon” to each temporal frequency and spatial wave number below a cutoff value fixed by  $k_i^{\text{max}} = \pi N_i / L_i$ . Grid parameters are chosen to ensure that in both real and Fourier space boundary reflection effects may be ignored. The numerical calculations assumed the following physical parameters  $\chi^{(2)} = 1.7 \times 10^{-12} \text{ mV}^{-1}$ ,  $\lambda = 1055 \text{ nm}$ ,  $n_1 = 1.604$ ,  $1/v_{g1} - 1/v_{g2} = -4.7 \times 10^{-11} \text{ s/m}$ ,  $2k_0^{(1)} - k_0^{(2)} = 500 \text{ m}^{-1}$ ,  $k_0^{(1)''} = 1.7 \times 10^{-26} \text{ s}^2/\text{m}$ ,  $k_0^{(2)''} = 8.9 \times 10^{-26} \text{ s}^2/\text{m}$ . We assume a FH Gaussian input beam with radial full width at half maximum (FWHM)  $w_0 = 35 \mu\text{m}$ , and temporal FWHM  $t_p = 1 \text{ ps}$ . The peak intensity  $I_0$  was varied up to values of tens of  $\text{GW}/\text{cm}^2$ . The grid parameters are  $L_x = L_y = 28.125 w_0 / r_0$ ,  $L_\tau = 6 t_p / t_0$  and  $N_x = N_y = 144$ ,  $N_\tau = 768$ .

Figure 3 summarizes the numerical results. The calculated output-beam diameters vs  $E_p/E_{TH}$  are presented in

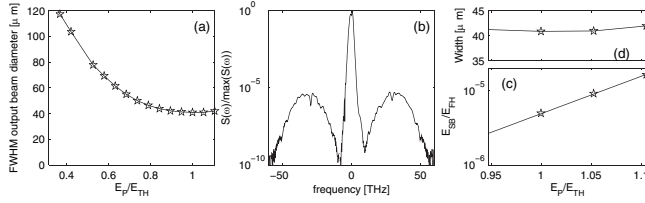


FIG. 3. Numerical results. (a) FWHM diameters of the FH output beams, vs threshold-normalized input-pump energy,  $E_p/E_{TH}$ ; (b) The spectrum of the FH field at the origin,  $S_{\mu}(\omega, x=0, y=0)/\max_{\omega,\mu} S_{\mu}(\omega, x=0, y=0)$ , for  $E_p/E_{TH} = 1.1$ . The spectrum is an average over  $\mathcal{N} = 8$  sample paths. (c) dependence of the fractional blue-sideband energy,  $E_{SB}/E_{FH}$ , on normalized pump energy. (d) magnified image of (a) over the same intensity range as (c). The calculations were limited to  $E_p/E_{TH} \leq 1.1$  due to memory limitations.

Fig. 3(a), where  $E_{TH} = 0.28 \mu\text{J}$ . By accounting for the given diameters and pulse durations, one obtains  $P_{\text{expt}}/P_{\text{theory}} = 1.32$  for the ratio between measured and calculated threshold powers. Furthermore, comparing the experimental [Fig. 1(a)] and calculated [Fig. 3(a)] output-beam diameters one should also notice the more abrupt dependence on pump energy, and the 1.45 times smaller diameter of the soliton at threshold, in the experimental case. These effects suggest the crystal has surface and/or bulk imperfections leading to linear and nonlinear spatial modulation of the input beam which are not included in the theory. On further testing we observed such beam distortions in the linear regime, and found a 30% change in the threshold power using a nominally identical crystal borrowed for testing purposes. Figure 3(b) shows the calculated FH spectral profile for  $E_p/E_{TH} = 1.1$ , which exhibits well-defined blue and red-shifted sidebands. The sidebands result from the amplification of vacuum fluctuations, and we have verified their absence in calculations in which this noise is set to zero. The sidebands have a width (at 1/10 of their peak) of  $\approx 18$  THz, in good agreement with the experiment. The frequency shift  $\Delta\Omega = 30$  THz, leading to  $\Delta\Omega_{\text{expt}}/\Delta\Omega_{\text{theory}} = 1.3$ . This discrepancy can be readily understood if one considers that, at threshold, one should expect  $I_{\text{expt}}/I_{\text{theory}} = 2.8$  for the ratio between soliton intensities, owing to the 1.32 times higher input power and the 2.1 times smaller output-beam area in the experiment. From the  $I\Delta\Omega^{-4}$  approximate scaling deduced from Eqs. (1) and (2) (in the limit of  $\Delta = 0$  and  $\delta k = 0$ ) one obtains  $\Delta\Omega_{\text{expt}}/\Delta\Omega_{\text{theory}} = 1.29$ . Figure 3(c) reports the calculated dependence of the output blue-sideband energy  $E_{SB}/E_{FH}$  relative to the pump component, in the vicinity of the soliton threshold. These energies were obtained by integrating the calculated FH field over appropriate apertures in direct and Fourier space. The results give  $E_{SB}/E_{FH} \approx 5 \times 10^{-6} - 2 \times 10^{-5}$  within 10% of the soliton threshold. These values are in good qualitative agree-

ment with the measured ones, given the uncertainty in system parameters.

In summary, we have captured the appearance of frequency sidebands in the spectra of  $\chi^{(2)}$  2D-spatial solitons near threshold. The result provides the first experimental confirmation of the temporal instability of  $\chi^{(2)}$  spatial solitons as predicted in Refs. [4,5]. By solving a quantum optical model that accounts for quantum field fluctuations, pump depletion, and diffraction/dispersion in  $3 + 1$  dimensions we obtain very good agreement between experiment and theory for sideband widths, frequencies, and energy content, if the pump power is scaled to the soliton-formation threshold. These results strongly support the contention that the instability seeding mechanism is quantum field fluctuations.

The authors acknowledge the support of the Italian Ministry of University and Research (MIUR) for the Grants No. FIRB01 and No. PRIN04. One of us (S.D.J.) thanks the Italian Fulbright Commission and the Institute of International Education for support. We thank R. Ballagh and G. Valiulis for discussions and L. Torner for discussions and the loan of an LBO crystal for testing purposes.

- 
- [1] F. Haake and R.J. Glauber, Phys. Rev. A **5**, 1457 (1972).
  - [2] F. Haake, Phys. Rev. Lett. **41**, 1685 (1978).
  - [3] V. Zakharov, Sov. Phys. JETP **24**, 4 (1967).
  - [4] A.A. Kanashov and A.M. Rubenchik, Physica (Amsterdam) **4D**, 122 (1981).
  - [5] A. De Rossi, S. Trillo, A.V. Buryak, and Y.S. Kivshar, Phys. Rev. E **56**, R4959 (1997).
  - [6] S.P. Gorza, N. Roig, P. Emplit, and M. Haelterman, Phys. Rev. Lett. **92**, 084101 (2004).
  - [7] D.V. Skryabin, Phys. Rev. E **60**, 7511 (1999).
  - [8] S. Minardi, J. Yu, G. Blasi, A. Varanavicius, G. Valiulis, A. Berzanskis, A. Piskarskas, and P. Di Trapani, Phys. Rev. Lett. **91**, 123901 (2003).
  - [9] W.E. Torruellas, Z. Wang, D.J. Hagan, E.W. VanStryland, G.I. Stegeman, L. Torner, and C.R. Menyuk, Phys. Rev. Lett. **74**, 5036 (1995).
  - [10] P. Zoller and P. Lambropoulos, J. Phys. B **12**, L547 (1979).
  - [11] P.D. Drummond, Phys. Rev. A **42**, 6845 (1990).
  - [12] M.G. Raymer, P.D. Drummond, and S.J. Carter, Opt. Lett. **16**, 1189 (1991).
  - [13] M.J. Werner and P.D. Drummond, Phys. Rev. A **56**, 1508 (1997).
  - [14] P.D. Drummond and S.J. Carter, J. Opt. Soc. Am. B **4**, 1565 (1987).
  - [15] M.J. Werner and P.D. Drummond, J. Comput. Phys. **132**, 312 (1997).
  - [16] A. Sinatra, Y. Castin, and C. Lobo, J. Mod. Opt. **47**, 2629 (2000).
  - [17] A. Sinatra, C. Lobo, and Y. Castin, J. Phys. B **35**, 3599 (2002).
  - [18] B.M. Caradoc-Davies, Ph.D. thesis, University of Otago, 2000.